

Luminosity Stability Issues for the TESLA Beam Delivery System (BDS)

*Nicholas Walker*¹ (DESY, Germany)

*Andrzej Wolski*² (Daresbury Laboratory, UK)

TESLA 2000-22
October 17, 2000

1 Introduction

Given the extremely small beam sizes required at the interaction point (IP) of the next generation of linear colliders, it has long been understood that particular attention must be made to component stability, in particularly with respect to ground motion and vibration. The beam deliver systems (BDS) contain some of the most tightest alignment tolerances of the entire machine. There have been many studies of the effects of ground motion and vibration in linear colliders both for TESLA and NLC/JLC (see for example [1,2]), and a recent review of stability issues for beam delivery systems can be found in [3]. In the TESLA conceptual design report (CDR) [4], studies of luminosity stability were made based on the so-called ATL ground motion model [5]. Since publication of the CDR, the TESLA BDS has undergone several major modifications:

- the undulator-based positron source has been incorporated up-stream of the main BDS;
- the energy and betatron collimation systems have been completely redesigned, and now includes the main emittance measurement section;
- the length of the final telescope has been increased from 130 m to 250 m, to accommodate the clean extraction of the beamstrahlung to the main dump hall.

gives the relevant TESLA parameters (500 GeV centre-of-mass version), and Figure 1.1 shows the new optics. Details of the lattice – and particularly the modifications – can be found in [6].

When talking about the effects of ground motion and vibration, it is important to separate out the various frequency-domains and their related effects. The luminosity loss itself can be separated into to two distinct mechanisms:

- beam-beam separation;
- increase in effective beam cross-section.

¹ email: nicholas.walker@desy.de

² current address: LBNL, Berkeley, CA. email: awolski@lbl.gov

Table 1.1: Relevant IP parameters
for TESLA-500

β_x		14 mm
β_y		0.4 mm
σ_x		500 nm
σ_y		5 nm
δ_{rms}^3	e^-	1.8×10^{-3}
	e^+	$\sim 4 \times 10^{-4}$
f_{rep}		5 Hz
N_b		2820
τ_b		337 ns

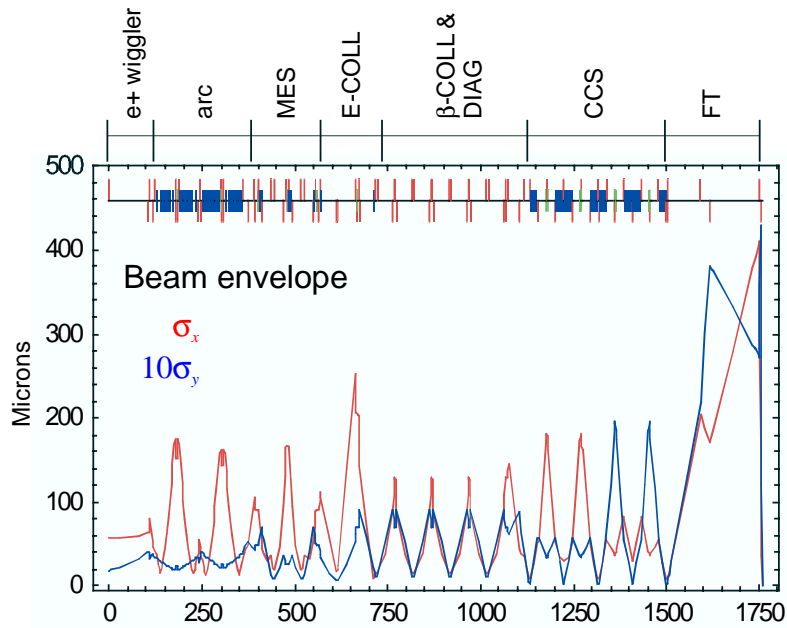


Figure 1.1: The TESLA BDS lattice (version 8).

The former tends to be the most critical, since the accumulated dipole kicks from misplaced magnets very quickly cause the beams to miss each other at the IP. Fortunately, the beams are effectively kept in collision by a fast IP intra-bunch feedback system, working in the 300 kHz range. The feedback system uses the first 20-100 bunches of the long TESLA bunch train (2820 bunches, with 337 ns spacing) to bring the remainder of the bunch train into collision. Since this effectively corrects independently each of the 5 Hz bunch trains, beam-beam separation due to magnet vibration and drift can be ignored. The fast feedback system and its performance is covered in detail elsewhere [7], and will not be considered further in this report. Instead we will concentrate on the increase in beam cross-section, which the fast feedback system cannot correct. Since $\sigma_y \ll \sigma_x$, we will consider only the effects in the vertical plane.

The beam size at the IP grows due to *aberrations* which are introduced by the beam going off-centre through the magnets of the entire BDS. The “orbit” is in turn driven by

³ Note that the large e^- energy spread is generated by the e^+ source undulator.

magnets being offset with respect to their design location. We can separate the various magnet motion effects into two time (frequency) intervals:

- fast motion ($> \sim 1$ Hz), which an orbit feedback system cannot correct, and
- slow drifts ($< \sim 1$ Hz), which the orbit feedback can follow.

The choice of cut-off frequency here depends primarily on the repetition rate of the machine. For TESLA, we have a 5 Hz rate, and so it is unlikely that an orbit correction feedback system could operate effectively above 1 Hz. To simplify the analysis, we assume that the “slow” motion is characterised by an ATL-like ground [5], where the variance of the relative displacement between two points separated by a distance L and after a time T is given by $\sigma_y^2 = ATL$, A being the constant of proportionality. From measurements of orbits at HERA, a conservative (upper-limit) on A for the DESY site is taken as $4 \times 10^{-6} \mu\text{m}^2\text{m}^{-1}\text{s}^{-1}$ [8], and this value will be used throughout the report. The “fast” motion is quantified by random uncorrelated RMS vibration of the magnets with an amplitude of 70 nm, a number which has been observed for frequencies above 2 Hz in the HERA tunnel [9].

In the following sections, we will reconsider the luminosity stability issues for the new TESLA BDS (version 8). Specifically, we will study

- effects of fast quadrupole vibration;
- magnet alignment tolerances;
- magnet field stability (and power supply tolerances);
- stabilisation against slow ground motion (ATL), including studies of BPM resolution and orbit feedback time-constant.

We begin with an analytical model using a thin-lens approach (section 2) and then report the results of tracking simulations, including a more realistic model for the orbit feedback correction (section 3.)

2 Analytical Approach

In previous studies, an analysis which takes into account a two-dimensional power spectrum ($P = P(\omega, k)$) based on semi-empirical studies and ground motion models have been used (see for example [1].) The power spectrum is folded into the lattice using the so-called *lattice response function* (see Appendix I). Here we adopt the less complex approach outlined in section 1:

- fast motion ($> \sim 1$ Hz) modelled as uncorrelated random motion with an amplitude of 70 nm RMS;
- slow drifts modelled as ATL-like motion, with $A = 4 \times 10^{-6} \mu\text{m}^2\text{m}^{-1}\text{s}^{-1}$.

2.1 Estimation of BDS Orbit due to quadrupole alignment errors

For simplicity, we model each quadrupole as a “thin-lens”, with an integrated strength $k = K_1 L$, where K_1 and L are the quadrupole strength (m^{-2}) and length respectively. In

addition, only kicks from quadrupoles are included: the dipole fields generated from offset sextupoles and octupoles are ignored.

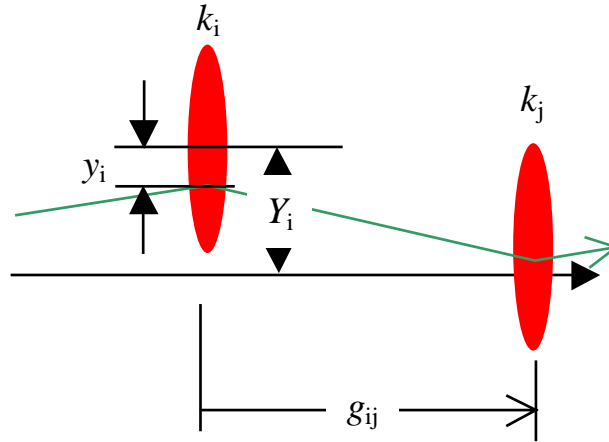


Figure 2.1: Thin lens analysis model.

Figure 2.1 introduces the notation, where

- k_i is the integrated quadrupole strength of the i^{th} magnet;
- Y_i is the offset of the i^{th} magnet with respect to some (arbitrary) reference line;
- y_i is the offset of the *beam* with respect to the i^{th} magnet centre;
- g_{ij} is the linear Greens function (R_{34} matrix term) from the i^{th} quadrupole to the j^{th} quadrupole ($j > i$).

By linear superposition, the beam offset at the i^{th} magnet is given by the sum of all the preceding kicks from the offset quadrupoles:

$$y_i = -\sum_{j=1}^i g_{ij} k_j Y_j - Y_i. \quad (1)$$

In keeping with convention, we assume that a positive k_i represents a *horizontally* focusing magnet (vertically defocusing). We can express equation (1) as a matrix equation:

$$\mathbf{y} = -\mathbf{Q} \cdot \mathbf{Y}, \quad (2)$$

where \mathbf{y} and \mathbf{Y} are vectors of the beam offsets (y_i) and quadrupole offsets (Y_i) respectively. \mathbf{Q} is the response matrix

$$\mathbf{Q} = \mathbf{G} \cdot \mathbf{diag}(\mathbf{k}) + \mathbf{I}, \quad (3)$$

where \mathbf{G} is the matrix of the linear Greens functions (g_{ij}), $\mathbf{diag}(\mathbf{k})$ is a diagonal matrix whose elements are the quadrupole strengths, and \mathbf{I} is the identity matrix. Note that \mathbf{G} and hence \mathbf{Q} are lower diagonal.

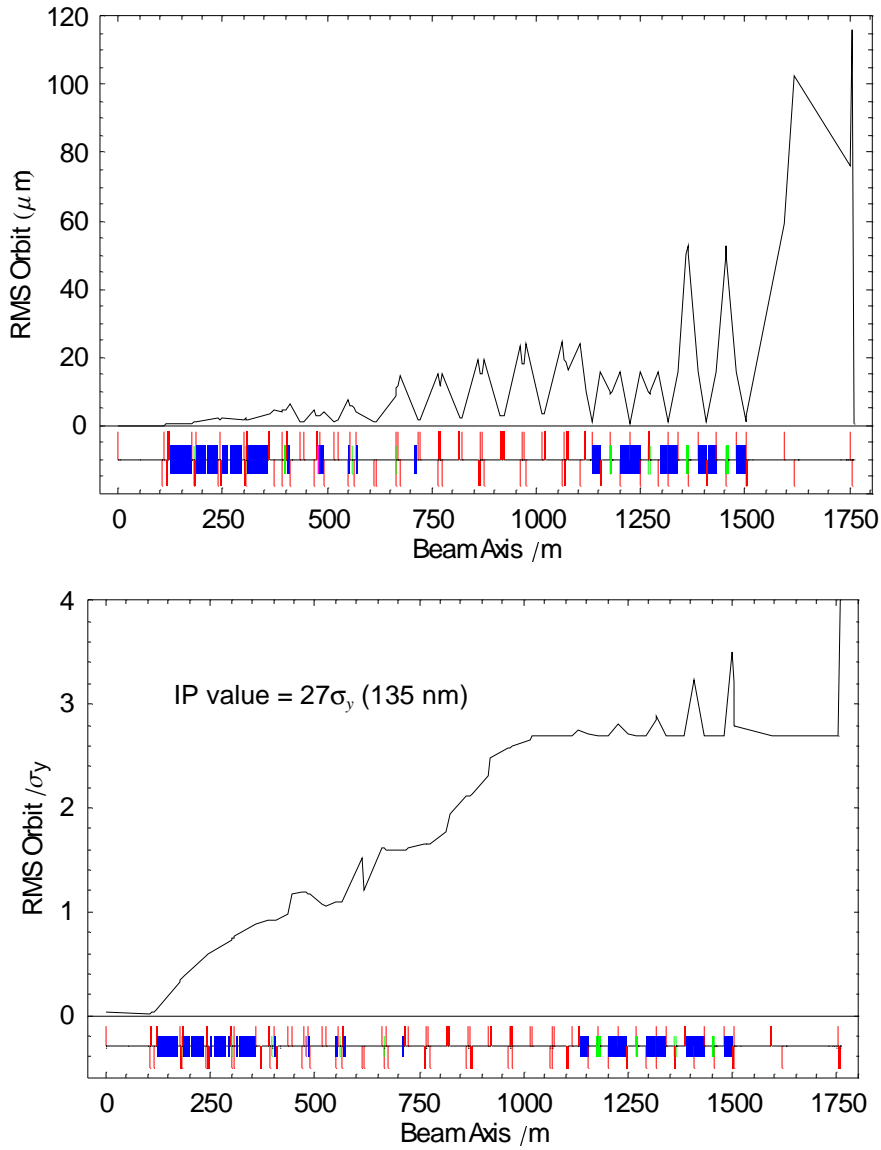


Figure 2.2: RMS orbit based on 70 nm of uncorrelated random quadrupole vibration. The top plot shows the RMS orbit in μm , while the bottom plot shows the RMS orbit normalised to the design beam size (σ_y).

2.2 RMS orbit

If we assume that each quadrupole has a BPM attached to it such that the electrical centre of the monitor is co-axial with the magnetic centre of the quad, then the vector \mathbf{y} in equation (2) can be thought of as a measured orbit. Given the statistical nature of the quadrupole offsets \mathbf{Y} , it is interesting to ask what the RMS orbit will be. From equation (1), it is straightforward to calculate the covariance matrix \mathbf{V}_y of the beam offsets (*i.e.* $\langle y_i y_j \rangle$):

$$\mathbf{V}_y = \mathbf{Q} \cdot \mathbf{V}_Y \cdot \mathbf{Q}^T, \quad (4)$$

where \mathbf{V}_Y is the covariance matrix of the quadrupole offsets ($\langle Y_i Y_j \rangle$). We must now ask what form \mathbf{V}_Y takes. We will look at two examples for the TESLA BDS system, namely uncorrelated quadrupole vibration (section 2.2.1), and then the so-called ATL ground motion model (section 2.2.2).

2.2.1 Random uncorrelated vibration

For uncorrelated motion, \mathbf{V}_Y becomes diagonal. Furthermore, if we assume that all the quadrupoles have the same RMS vibration amplitude (σ_Y), then we can write $\mathbf{V}_Y = \sigma_Y^2 \cdot \mathbf{I}$. Equation (4) then simplifies to

$$\mathbf{V}_y = \sigma_Y^2 \mathbf{Q} \cdot \mathbf{Q}^T. \quad (5)$$

Figure 2.2 shows the results for $\sigma_Y = 70$ nm vibration. The normalised RMS (bottom figure) increases steadily over the initial 1000 m of beamline, up to a relatively constant value of approximately $3\sigma_Y$ across the FFS. The behaviour reflects the fact that nearly all the quadrupoles in the FFS are effectively at the same phase; thus they tend only to influence the motion at the IP (which is at the orthogonal phase), and contribute little to the RMS in the FFS itself. The spikes are located at those magnets close to the IP image points, which sample the IP phase. The RMS value at the IP is approximately $27\sigma_Y$ (or 135 nm). The large increase is primarily due to the final doublet quadrupoles, which in this analysis are also vibrating independently with an amplitude of 70 nm.

Figure 2.2 represents only the diagonal terms of the covariance matrix \mathbf{V}_y . It is also interesting to look at the off-diagonal terms, since they indicate the correlation of the beam motion. Figure 2.3 shows correlation matrix of \mathbf{V}_y graphically as a density plot.

The plot shows that the ‘‘orbit’’ becomes strongly correlated in the downstream sections (*i.e.* the FFS). This reflects the coherent betatron oscillation that has accumulated over the initial part of the BDS due to the random quadrupole vibrations. As we have previously noted, the FFS quadrupoles themselves will have little influence on this oscillation, except in the orthogonal (IP) phase. It is interesting to note, therefore, that the forseen fast feedback system which will be placed just upstream of the FFS will effectively cancel the downstream $3\sigma_Y$ jitter in that region. In the upstream regions, however, such a relatively large amplitude pulse-to-pulse jitter may have implications for orbit correction and beam based alignment. We should also note here that the fast feedback system will at least require a bunch train of a few tens of bunches to function.

2.2.2 A·T·L ground motion

ATL is an empirical law which has been successfully used to predict the effects of longer term ground motion on linear colliders. It states that after a time T , the variance of the relative offset of two points separated by a distance L is proportional to both L and T [5]:

$$\sigma_Y^2 = A \cdot T \cdot L. \quad (6)$$

The constant A has been measured for the DESY site [8], and has the approximate value $4 \times 10^{-6} \mu\text{m}^2 \text{m}^{-1} \text{s}^{-1}$. The question now is what form the covariance matrix \mathbf{V}_Y in equation 4 has when considering ATL-like motion. If the longitudinal beam axis location of the i^{th} magnet is z_i , then it can be show (Appendix II) that the covariance matrix has the form:

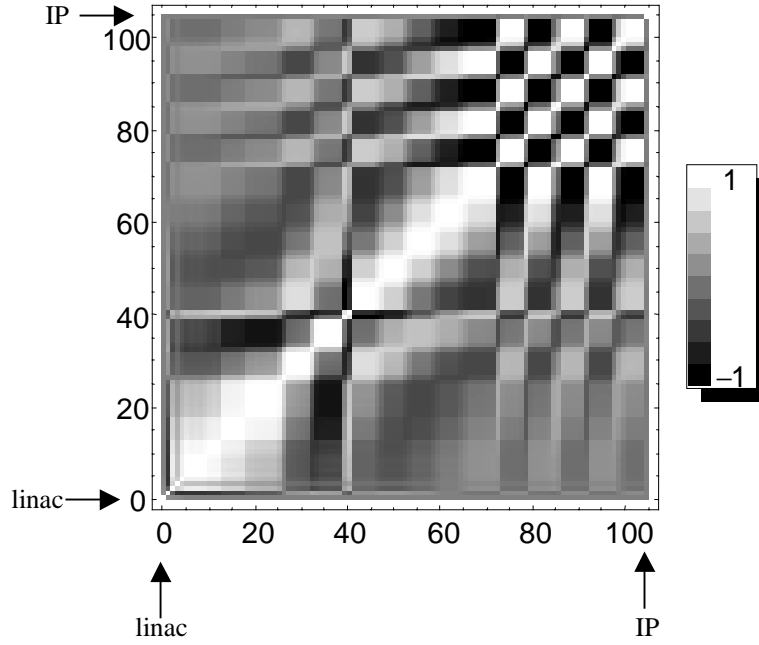


Figure 2.3: Correlation between quadrupole-beam offsets (orbit). Note that the orbit in the FFS (Nos. 70-105) is completely correlated.

$$\mathbf{V}_Y = A \cdot T \cdot \begin{pmatrix} z_1 & z_1 & z_1 & \dots \\ z_1 & z_2 & z_2 & \dots \\ z_1 & z_2 & z_3 & \dots \\ \vdots & \vdots & \vdots & \ddots \end{pmatrix} \quad (7)$$

From equation 7, we can see that the variance of the i^{th} magnet offset with respect to the beamline origin $z = 0$, is given by $\langle Y_i^2 \rangle = A \cdot T \cdot z_i$, which is in accordance with equation (6). The *covariance* between two magnet offsets is given by $\langle Y_i Y_j \rangle = A \cdot T \cdot z_i$, for $z_i < z_j$ ⁴. This is typical for random walk behaviour, of which ATL is an example. Unlike the bounded quadrupole vibration dealt with earlier, the expected RMS of the orbit motion with ATL increases with \sqrt{T} . In addition, there is a significant difference in what is meant by RMS here. For the uncorrelated quadrupole vibration, the calculated RMS plotted in Figure 2.2 represents a physical quantity that we could measure by talking many consecutive pulses, measuring the orbits and then calculating the RMS. The result should look like Figure 2.2, assuming of course that we have 70 nm of uncorrelated quadrupole vibration. For ATL, the RMS calculated by inserting equation (7) into (4), reflects more the statistical probability of a given orbit after T seconds of ATL-like ground motion. One interesting question to ask is how long is required before the orbit due to ATL ground motion is comparable to the RMS jitter due to the random quadrupole vibration. Figure 2.4 shows both the normalised quadrupole vibration RMS and the ATL RMS, the later scaled to match (in the least-square sense) the former. We

⁴ Implicit here is the assumption that all z_i have positive values.

find that it requires 358 seconds, or six minutes, before both RMS envelopes match⁵ (Figure 2.4).

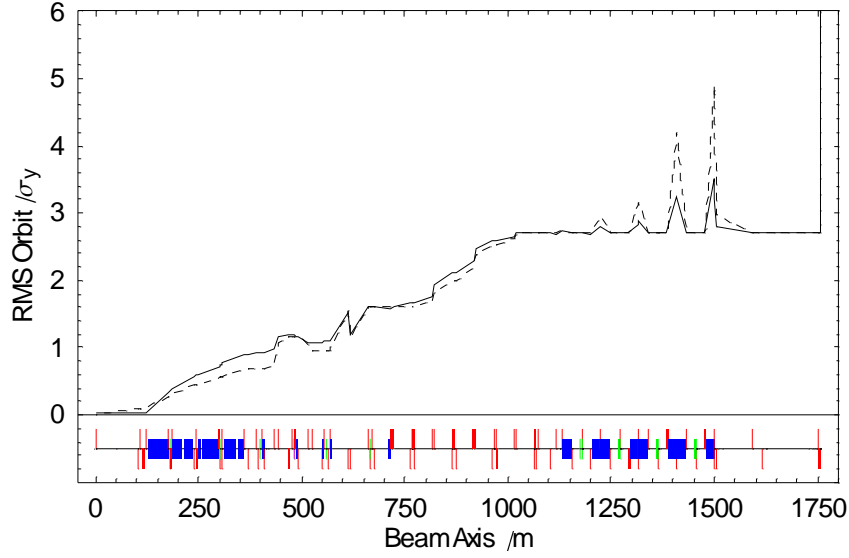


Figure 2.4: Comparison of RMS orbits generated by ATL ground motion after ~6 minutes (dashed), and 70 nm random quadrupole vibration (solid).

2.3 Effects of orbit distortion on σ_y^*

We are now in a position to estimate the effects of magnet motion – and the resulting orbit – on the vertical beam size at the IP (σ_y^*). To first-order in the kick strength, there are two main (linear) aberrations that we need to consider, dispersion and cross-plane coupling⁶. Table 2.1 summarises the aberrations, their sources and their associated Lie generators.

Table 2.1: Linear Aberrations and their associated sources and Lie generators.

magnet type	aberration type	generator	IP generator
quadrupole	dispersion	$k_i y_i y \delta$	$-k_i y_i R_{34} y' \delta$
sextupole	dispersion	$-s_i D_x y_i y \delta$	$s_i D_x y_i R_{34} y' \delta$
sextupole	x - y coupling	$-s_i y_i x y$	$-s_i y_i R_{12} R_{34} x' y'$

All the terms are linear in the beam offsets y_i . The total generator can be estimated (to first-order in the kick strengths) as a sum of all the IP generators. Following our matrix style, we define a vector \mathbf{D} such that

$$\mathbf{D} = (\mathbf{s} \circ \mathbf{D}_x - \mathbf{k}) \circ \mathbf{R}_{34} \quad (8)$$

where

⁵ This value is really only of academic interest, since the validity of ATL over such a short time range is very questionable.

⁶ In principle, we should also consider the vertical waist shift term y'^2 ; however, this would require a horizontal offset in a sextupole magnet, which is not included in this analysis.

- \mathbf{s} is a vector of the integrated sextupole strengths (m^{-2});
- \mathbf{k} is a vector of the integrated quadrupole strengths (m^{-1});
- \mathbf{D}_x is a vector of the dispersion function at each magnet, and
- \mathbf{R}_{34} is a vector of the vertical Greens function from each magnet to the IP.

The symbol \circ denotes element-wise multiplication. Similarly for the coupling, we define a vector \mathbf{C} :

$$\mathbf{C} = -\mathbf{s} \circ \mathbf{R}_{12} \circ \mathbf{R}_{34} \quad (9)$$

\mathbf{R}_{12} being the corresponding vector of horizontal Greens functions from the magnet to the IP. The RMS vertical IP dispersion can then be obtained as

$$\begin{aligned} D_{y,RMS}^2 &= \mathbf{D} \cdot \mathbf{V}_y \cdot \mathbf{D}^T \\ &= (\mathbf{D} \cdot \mathbf{Q}) \cdot \mathbf{V}_Y \cdot (\mathbf{D} \cdot \mathbf{Q})^T \end{aligned} \quad (10)$$

For the 70 nm uncorrelated quadrupole vibration, we obtain $D_{y,RMS} \approx 1.7 \mu\text{m}$. For the *electron* beam, the energy spread is approximately 1.8×10^{-3} , which corresponds to an RMS vertical beamsize increase of ~ 3 nm, added in quadrature with the nominal design value of 5 nm. This corresponds to an RMS luminosity loss of

$$\frac{\Delta L}{L} \approx -\frac{1}{4} \left(\frac{\Delta \sigma_y}{\sigma_y} \right) \approx -9.5\% . \quad (11)$$

Because we need only consider one beam (the electrons), we replaced the usual numerical factor of $1/2$ by $1/4$ (the contribution from the positron beam with an energy spread of approximately 4×10^{-4} can be ignored.)

The total coupling generator can be estimated in a similar manor:

$$C_{RMS}^2 = (\mathbf{C} \cdot \mathbf{Q}) \cdot \mathbf{V}_Y \cdot (\mathbf{C} \cdot \mathbf{Q})^T \quad (12)$$

Again for an uncorrelated quadrupole vibration of 70 nm, we find $C_{RMS} \approx 41 \mu\text{m}$. The nominal horizontal beam divergence is $37 \mu\text{rad}$, which corresponds approximately to 1.5 nm added in quadrature to the vertical beam size. Unlike the dispersion, we must now consider both electron and positron beams, so the average reduction in luminosity is

$$\frac{\Delta L}{L} \approx -\frac{1}{2} \left(\frac{\Delta \sigma_y}{\sigma_y} \right)^2 \approx -4.5\% \quad (13)$$

Taking both the contributions from dispersion and coupling into account gives approximately 14% total average luminosity loss, for 70 nm uncorrelated quadrupole vibration. A luminosity loss of 2% would therefore require a vibration tolerance of some $70/\sqrt{7} \sim 26$ nm.

For ATL-like ground motion, we can use the above analysis to estimate the time between successive orbit corrections. For $A = 4 \times 10^{-6} \mu\text{m}^2 \text{m}^{-1} \text{s}^{-1}$, we find that

$$D_{y,RMS} [\mu\text{m}] \approx 0.12 \times \sqrt{T}$$

and

$$C_{RMS} [\mu\text{m}] \approx 3.6 \times \sqrt{T}$$

The corresponding average luminosity loss is

$$\frac{\Delta L}{L_{ATL}} \approx -8 \times 10^{-4} T$$

Thus, an average 10% luminosity loss requires approximately 125 seconds, or two minutes. In the real machine we expect to have a continuous feedback orbit correction, running at something on the order of 0.1Hz (section 3.4): hence the luminosity loss due to ATL should be reduce to the order of 1% or less, until either the dispersion generated from the corrector magnets (see section 2.6) or ultimately non-linear aberrations begin to dominate.

2.4 Effects of Second-Order Dispersion

Second-order dispersion is generated when linear dispersion is transported through a chromatic section. We can use the above formalism to estimate the second-order dispersive effects by first calculating the linear dispersion at each magnet (\mathbf{D}_y), and then effectively use this result as the “orbit” in the previous linear dispersion calculation.

We must first calculate the dispersion vector at each magnet (not just at the IP as in section 2.3). We use a modified form of equation 8:

$$\Delta = (\mathbf{s} \circ \mathbf{D}_x - \mathbf{k}) \cdot \mathbf{G} \quad (14)$$

where \mathbf{G} is the matrix of vertical linear Greens functions (g_{ij} , see equation 3), and consequently Δ is also a matrix⁷ (both being lower diagonal). For a given “orbit” vector \mathbf{y} , the vertical dispersion at each magnet is given by the vector \mathbf{D}_y :

$$\mathbf{D}_y = \Delta \cdot \mathbf{y} \quad (15)$$

The second-order dispersion generates at the IP (η_y) is then given by

$$\eta_y = \mathbf{D} \cdot (\Delta \cdot \mathbf{y}) \quad (16)$$

As before, we can estimate the RMS second-order dispersion σ_{η_y} :

$$\begin{aligned} \sigma_{\eta_y}^2 &= (\mathbf{D} \cdot \Delta) \cdot \mathbf{V}_y \cdot (\mathbf{D} \cdot \Delta)^T \\ &= (\mathbf{D} \cdot \Delta \cdot \mathbf{Q}) \cdot \mathbf{V}_Y \cdot (\mathbf{D} \cdot \Delta \cdot \mathbf{Q})^T \\ &= \mathbf{\Gamma} \cdot \mathbf{V}_Y \cdot \mathbf{\Gamma}^T \end{aligned} \quad (17)$$

where the vector $\mathbf{\Gamma} = \mathbf{D} \cdot \Delta \cdot \mathbf{Q}$ is only a function of the lattice. Again, for random uncorrelated quadrupole vibration we have

⁷ Note that the last row of Δ is our original \mathbf{D} vector in equation 8.

$$\sigma_{\eta_y}^2 = \sigma_Y^2 \Gamma \cdot \Gamma^T. \quad (18)$$

For the BDS and $\sigma_Y = 70$ nm, we obtain

$$\sigma_{\eta_y} \approx 543 \mu\text{m}.$$

In the case of second-order dispersion, an energy spread gives rise to a shift in the beam centroid ($= \eta_y \delta_{rms}^2$). Again, considering only the electron beam energy spread of $\delta_{rms} = 1.8 \times 10^{-3}$, we find a RMS centroid shift of ~ 1.8 nm. This centroid shift is assumed to be corrected by the fast feedback system. The RMS addition to the beam size is $\sqrt{2}$ times the centroid shift (see Appendix III). Hence for second-order dispersion we have

$$\Delta\sigma_y \approx 2.5 \text{ nm}$$

added in quadrature to the design 5 nm. Note that this effect is comparable to that of the linear dispersion (~ 3 nm) calculated in section 2.3. From equation 11, the non-linear dispersion generates a further $\sim 6.5\%$ loss in luminosity.

2.5 Summary of luminosity loss due to fast quadrupole vibration

Table 2.1 summarises the results for the fast quadrupole vibrations, based on the previous analysis.

Table 2.2: Summary of luminosity loss contributions from 70 nm of random uncorrelated quadrupole vibration.

Aberration	contribution to $\Delta L/L$	Comments
x - y coupling	4.5%	both beams
linear dispersion	9.5%	e^- only
2 nd -order dispersion	6.5%	e^- only
total	20.5%	

The total loss of 20.5% is rather high. However, one should bear in mind that the effect scales as the square of the RMS vibration amplitude (σ_Y^2), and that an RMS vibration of 70 nm above ~ 0.1 Hz is probably conservative⁸. An RMS vibration of 20 nm would result in $<2\%$ loss. Such values have been measured at “quiet sites” (FFTB at SLAC), and in addition it has been shown that 20 nm can be achieved using active-piezo stabilisation (feedback) on the quadrupoles [10]. In addition, the assumption of no correlation at these amplitudes is also pessimistic (see Appendix I.)

2.6 Estimate of tuning time for one-to-one orbit correction

We now estimate the mean time before the dispersion generated by a one-to-one steering algorithm under the influence of ATL-like motion significantly degrades the luminosity. We will refer to this time as the *mean tuning time*, since it reflects the average time between performing semi-invasive correction of the vertical IP dispersion.

⁸ We assume that the orbit correction feedback should be able to correct frequencies below 0.1 Hz.

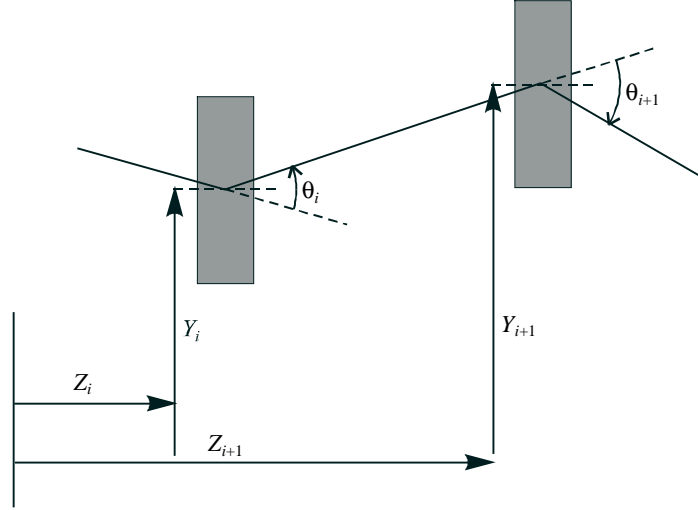


Figure 2.5: *Simplistic one-to-one steering model.*

Figure 2.5 shows our simplified model of one-to-one steering. In the analysis, we make the following assumptions (approximations):

- each magnet has a vertical corrector dipole at its location;
- each magnet has a perfect (no noise) BPM mechanically aligned to its centre;
- the beam is steered *exactly* to the BPM zero, and hence through the centre of each magnet, using the upstream corrector.

Since the beam by definition passes through the centre of each magnet, no spurious dispersion or coupling is generated. Only the dispersive kick from each of the correctors remains. The magnitude of the dispersion is given by the angle. From Figure 2.5, we can see that the (angular) dispersion generated by the i^{th} corrector is

$$D'_i = -\theta_i \approx -\left(\frac{Y_{i+1} - Y_i}{z_{i+1} - z_i} - \frac{Y_i - Y_{i-1}}{z_i - z_{i-1}}\right) \equiv -\left(\frac{\Delta Y_{i+1}}{\Delta z_{i+1}} - \frac{\Delta Y_i}{\Delta z_i}\right). \quad (14)$$

The total vertical IP dispersion is

$$D_y = \sum_i -\left(\frac{\Delta Y_{i+1}}{\Delta z_{i+1}} - \frac{\Delta Y_i}{\Delta z_i}\right) g_i = \sum_i \frac{\Delta Y_i}{\Delta z_i} (g_i - g_{i-1}), \quad (15)$$

where g_i is the linear Greens function from the magnet to the IP (note that $g_0 \equiv 0$). For ATL-like motion, the ΔY_i are uncorrelated and the RMS is given by $AT\Delta z_i$. Hence

$$D_{y,RMS}^2 = AT \sum_i \frac{(g_i - g_{i-1})^2}{\Delta z_i}. \quad (16)$$

For the BDS, again assuming $A = 4 \times 10^{-6} \mu\text{m}^2 \text{m}^{-1} \text{s}^{-1}$, we find

$$D_{y,RMS} [\text{nm}] \approx 4.2 \times \sqrt{T}.$$

Thus for an RMS electron beam energy spread of 1.8×10^{-3} , we would achieve a 10% luminosity loss after a mean time of approximately 50 hours.

3 Simulation (Particle Tracking) Results

Given the complexity of a linear collider beam delivery system, it is necessary to confirm the analytical results obtained in section 2 with simulations accounting for as many of the various effects as possible. In section 3.1, we consider vertical alignment tolerance for single magnets. Section 3.2 deals with the sensitivity of individual magnet field strengths, while section 3.3 calculates the magnet power supply stability requirements. In section 3.4, we consider a more realistic dynamic model, in which the effects of a feedback system (orbit correction) is also included. The results presented here will give an indication of the required tolerances in magnet alignment, power supply stability and BPM resolution.

The tracking was performed using a BDS model constructed with the MERLIN-II class library [11]. Typically 500 particles were tracked, using the same initial distribution for each simulation run, thus avoiding statistical fluctuation effects due to initial beam samples. The tolerance is defined as the variation leading to a 2% loss in luminosity from an increase in the vertical beam size (no beam-beam effect). In all cases, it is assumed that any associated beam-beam offset would be completely corrected by the IP fast feedback system, and is therefore ignored.

3.1 Single Magnet Alignment Tolerance

The tolerances were determined by recording the beam size relative to design value, as each element in turn was moved vertically in steps from 0 to 1 μm . The data of relative luminosity versus vertical alignment were fitted with a third order polynomial, which was solved to find the alignment giving 98% of nominal luminosity. The sensitivity is simply the reciprocal of the tolerance.

Alignment sensitivities for the quadrupoles are shown in Figure 3.1, and for the sextupoles in Figure 3.2. In the case of the quadrupoles (Figure 3.1), the results of the tracking simulations are compared with analytical estimates based on the models developed in section 2. The analytical calculation includes the effects of both the linear terms and non-linear dispersion. The agreement between simulation and analytical calculation is very good, showing that there are no additional major aberrations beyond those already considered.

The majority of quadrupoles allow a displacement greater than 0.1 μm before resulting in a 2% luminosity loss, although a significant number have a tolerance below 0.1 μm . As might be expected, the sextupole displacements having the largest effect on the vertical beam size are those in the vertical chromatic correction section, where the sextupole strengths and vertical beta functions are large. It is clear that the requirements on initial magnet positioning are very demanding, and that an effective orbit correction system will be essential for maintaining good luminosity.

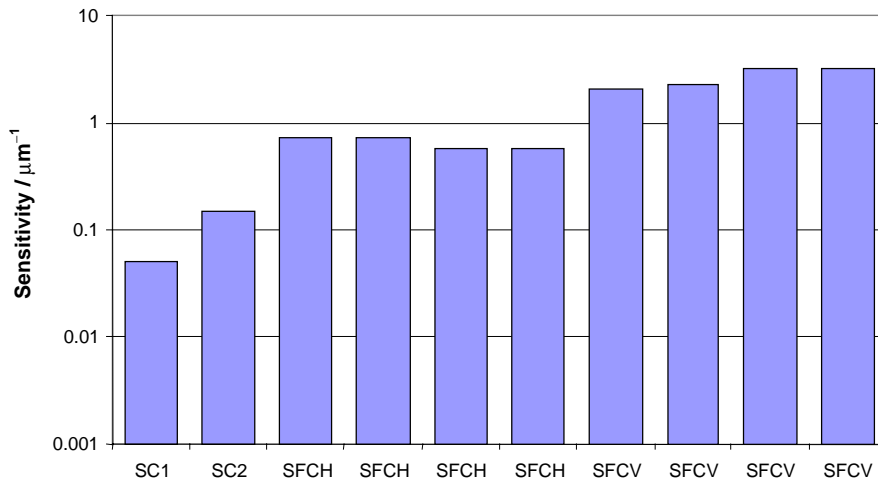


Figure 3.2: Vertical alignment sensitivity for the BDS sextupoles (2% luminosity reduction).

3.2 Single Magnet Field Stability

Figure 3.3 shows the luminosity sensitivity to variation of the sextupole field gradient, and Figure 3.4 shows the corresponding sensitivity for the quadrupoles. Here, the tolerance is defined as the relative gradient variation leading to a 2% luminosity loss, and as before the sensitivity is the reciprocal of the tolerance.

3.3 Power Supply (Circuit) Tolerances

While the results presented in Figure 3.3 and Figure 3.4 show us which specific magnets have high sensitivities, an important tolerance is that on the power supply stability used to drive these magnets. A single power supply may be used to drive several magnets in a string (circuit), and in this case the resulting correlation must be taken into account.

Where possible, the magnets in the BDS (including dipoles) were grouped into families where a single power supply could be used to drive them. These “circuits” were then constructed in the MERLIN-II model, and the sensitivities were calculated as before, the only difference being that now the power supply was adjusted rather than the field of the individual magnets.

In order to calculate a set of power supply tolerances from the simulation results, the following steps were taken:

1. a tolerance for each power supply was estimate based on a 2% luminosity loss;
2. the set of tolerances were grouped into sensitivity decades;
3. each decade set was scaled (weighted by the number in the set) so that the *total* estimate loss was 2%.

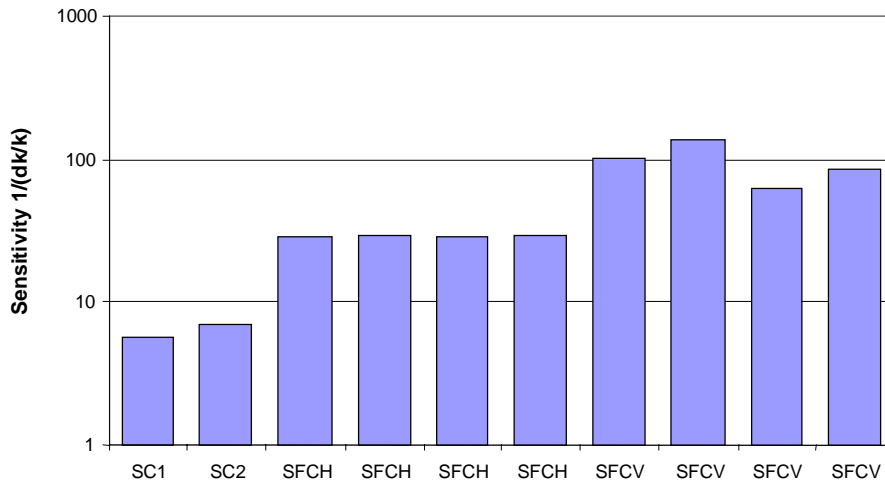


Figure 3.3: Luminosity sensitivity to sextupole field variation in the TESLA BDS. The bar heights show the reciprocal of the field variation giving 2% loss in luminosity from spot size increase at the IP.

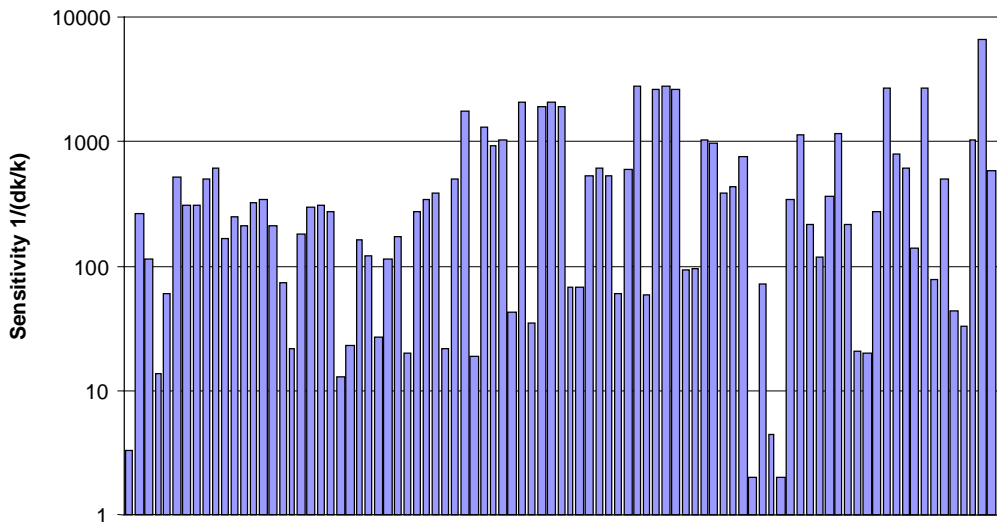


Table 3.1: Power supply tolerances (stability) estimated from tracking simulations.
The total luminosity loss is of the order of $\sim 3\%$

Stability	# PS	magnets	magnet type	# magnets
10^{-4}	41			80
5.10^{-5}	6	BCMES1	dipole	2
		BCMES3	dipole	2
		QCBC1	quad	8
		QCBC2	quad	8
		QFC2	quad	7
		QFT3	quad	1
10^{-5}	5	S.C. Doublet	quad	2
		BFCV	dipole	40
		BFCH	dipole	40
		BLPA	dipole	48
		BLNA	dipole	48
total supplies	52		total magnets	286

3.4 ATL Ground Motion and (Slow) Feedback System Simulations

In section 2.3 it was estimated that ATL-like ground motion would cause an average luminosity loss of some 10% after ~ 100 seconds, assuming that the beam-beam separation is corrected by the IP fast feedback system. It will thus be necessary to correct the overall orbit in the BDS on a continuous basis in order to compensate the effects of the ground motion. For the purposes of this study we assume a simple one-to-one steering algorithm, where an upstream ‘‘corrector’’ is effectively used to correct the beam offset at the downstream magnet. The one-to-one algorithm is not dispersion free, and in section 2.6, it was estimated that the correction would result in a average luminosity loss of 10% after ~ 50 hours, which is a gain of three orders of magnitude in stability.

Ground motion effects have been added to MERLIN-II, that will displace supports according to the ATL model. For our simulations, a system of girders was set up to support all elements in the beam delivery system, with BPMs and correctors fixed with respect to the adjacent magnet. The model is simplified in that only vertical movements of each girder are allowed, with all elements on any one girder in fixed positions relative to one another. 105 BPMs and a corresponding number of correctors were used, distributed from the end of the main linac to just upstream of the final doublet. The feedback system simulation uses a straightforward singular value decomposition (SVD) of the response matrix to determine the required corrector strengths from the BPM

readings. The system is assumed to operate on a pulse-to-pulse basis, so BPM readings are found and corrector strengths determined by tracking through the BDS, then 0.2 seconds of ATL ground motion is applied, before a further tracking run to determine the actual beam size at the interaction point. The two fast kickers for the intra-bunch-train feedback system [7] were also included, although no dynamic effects of this system were modelled (the IP angle and bunch offset were always exactly corrected without error.)

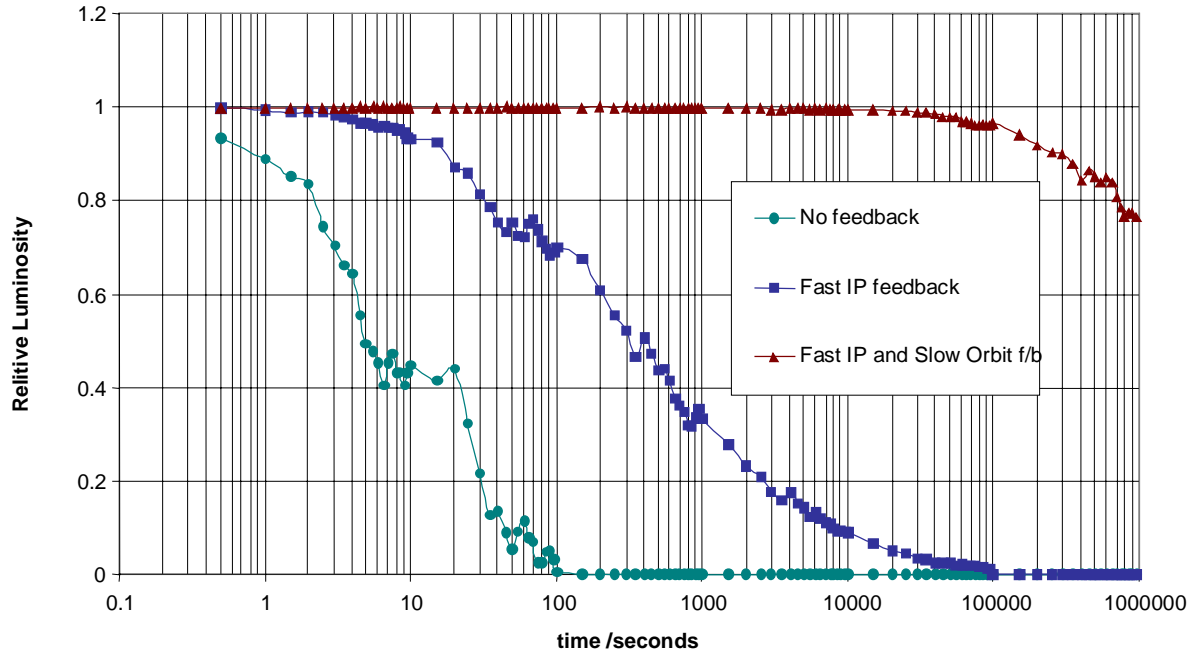


Figure 3.5: Effect of feedback systems on luminosity. The feedback systems are assumed to operate without BPM noise. The ground motion was modelled using ATL with $A = 4.1 \times 10^{-6} \mu\text{m}^2/\text{m/s}$. The graph shows the results of averaging over 20 seeds of random ground motion.

The results of the simulations are shown in Figure 3.5. Without feedback systems, the luminosity falls to zero after about 100 s as the two beams move apart. When the fast IP feedback is applied and the beams are kept in collision, the luminosity takes longer to fall, but is still reduced by 10% after about 20 seconds by growth of the beam size due to coupling and dispersive effects: this result disagrees with our original analytical estimate of ~ 100 seconds (section 2.3). With fast IP and slow orbit feedback (no BPM noise), the luminosity is held very stable up to about 3 hours, and then starts to fall, though is still at the 95% level after a day of operation. Here the loss of luminosity due to the dispersive nature of one-to-one steering agrees much better with the predictions of the analytical treatment given in section 2.6.

The results shown in Figure 3.5 assume no additional noise on the BPM measurements. The effects of BPM noise are shown in Figure 3.6. The data were obtained by simulating operation of the feedback systems over 200 seconds (1000 pulses), and finding the mean relative luminosity. Again, the fast IP feedback is applied as a perfect correction. Each curve on the graph shows different amounts of BPM noise on the slow orbit feedback system, with gain varying from 1 to 2×10^{-3} (the time constant is just the reciprocal of the product of gain and pulse repetition rate). With unit gain applied

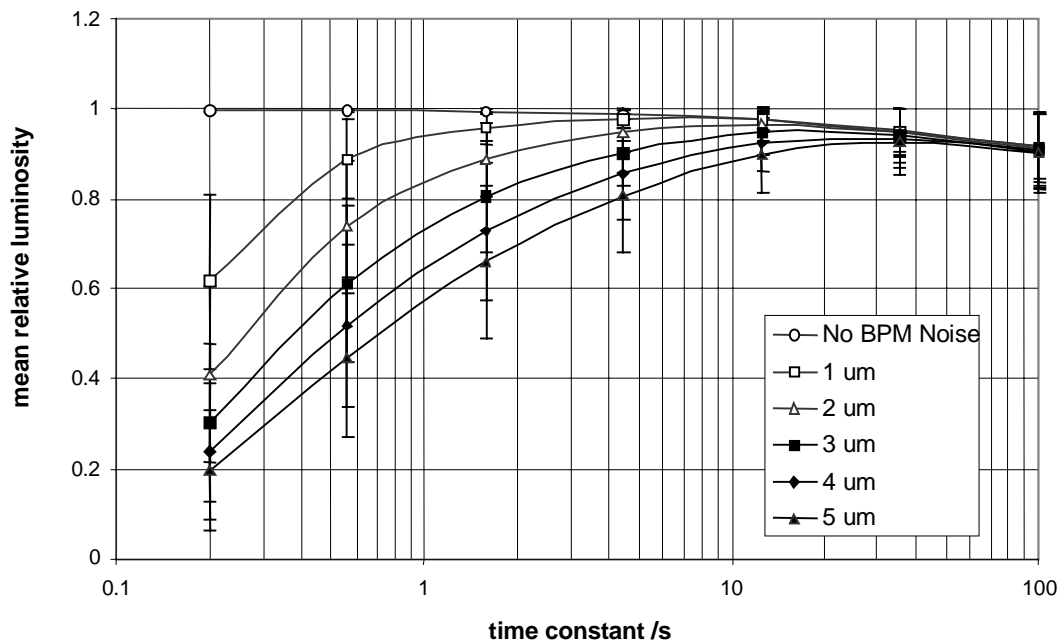


Figure 3.6: Relative luminosity averaged over 200 seconds as a function of the feedback system time constant. The curves show results for increasing amounts of BPM noise.

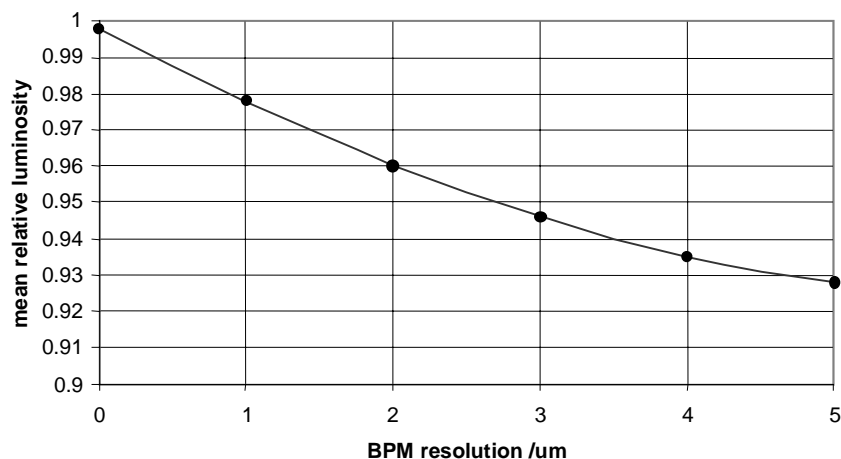


Figure 3.7: Maximum achievable relative luminosity as a function of BPM noise. The optimum feedback time constant is selected in each case.

($\tau = 0.2$ s), the presence of $1 \mu\text{m}$ BPM noise reduces the luminosity by around 40%. Reducing the gain effectively improves the BPM resolution by averaging over a number of pulses, and the luminosity curve peaks at an optimum gain. Beyond this point, the longer time constant prevents the feedback from keeping up with the ATL ground motion, and the luminosity starts to fall off. Figure 3.7 shows how the maximum relative luminosity falls off with increasing BPM noise. Even with $3 \mu\text{m}$ BPM noise, it is possible to achieve close to 95% mean luminosity. For TESLA, we have specified a $1 \mu\text{m}$ BPM resolution, which should enable us to run the orbit correction with a time constant of 4 s (0.25 Hz), and still have only a few percent luminosity loss.

4 Summary

Table 4.1 summarises the total contributions to luminosity loss for the TESLA BDS considered in this report. The total loss of ~26% is dominated from the 70 nm fast quadrupole motion. However, as we pointed out in section 2.5, these effects scale quadratically with vibration amplitude, and magnet stabilisation at the level of 20 nm RMS has been achieved using fast piezo stabilisation feedback. It should also be noted that the figure of 20.5% was arrived at assuming completely uncorrelated random vibration, which is almost certainly pessimistic (see Appendix I.) For a better estimate, a more complex model of the vibration spectrum (including correlation between near-neighbour quadrupoles) must be made (as in [1,2].) However, such calculations ultimately require the measurement of the exact spectrum of the quadrupole vibration as input, and that is difficult to estimate with any precision until the machine is actually built. However, from existing measurements in the HERA tunnel, it would seem that 70 nm uncorrelated motion is a conservative number, and indeed there exists measurements that suggest a more modest ~40 nm [9]: this alone would reduce the fast vibration contribution to ~7%.

Table 4.1: Summary of luminosity stability (loss) contributions from the sources considered

Source		contribution to $\Delta L/L$	Comments
<i>Fast (>2Hz) quad vibration (70 nm RMS)</i>	<i>Aberration:</i>		
	<i>x-y coupling</i>	4.5%	both beams
	<i>linear dispersion</i>	9.5%	e ⁻ only
	<i>2nd-order dispersion</i>	6.5%	e ⁻ only
	<i>total</i>	20.5%	
<i>Power supply stability</i>		3%	
<i>Slow Orbit feedback (ATL)</i>		2%	
TOTAL		~26%	

For slow drifts (ATL), a one-to-one steering algorithm is sufficient to stabilise the average luminosity over a few days, until a semi-invasive dispersion correction needs to be made. The time could in principle be extended by using a better – dispersion free – steering algorithm. One such possible algorithm would be to adjust the orbit asymmetrically in the vertical CCS sextupole pairs to generate dispersion at the IP which would compensate the dispersion generated by the correctors. The mean tuning time would then be defined by the second-order dispersion generated. Such algorithms will be the subject of further study.

Appendix I Lattice response function

In much of the literature on ground motion and its effect on beam stability in beam delivery systems, use of a lattice response function is made (see for example [1,2].) The response function shows the response of the IP beam offset and cross-section as a function of $k = 2\pi/\lambda$ of the ground motion waves. With the exception of the ATL-like motion, we have ignored the correlation between magnets, and have effectively taken the short-wavelength limit of the ground motion.

To calculate the response function, we need only calculate the corresponding covariance matrix \mathbf{V}_Y for a simple harmonic wave:

$$\langle Y_i Y_j \rangle = \frac{A^2}{2} \cos(k(z_j - z_i)) \quad (\text{I.1})$$

where A is the amplitude of the wave, and z_i and z_j are the locations of the i^{th} and j^{th} magnets respectively. In the long-wavelength limit, the motion corresponds to a uniform offset of all the magnets; this effectively represents an offset of the beam at the entrance to the system, and so the resulting IP offset would be $-R_{33}Y$, where R_{33} is the cosine-like response of the entire beamline, and Y is the offset. Such an offset is unrealistic, since at very long wavelengths (low frequencies), one would assume that the beam is injected on the displaced axis of the beamline⁹. If \mathbf{Q}_{ip} is a vector corresponding to the last row of our previous response matrix \mathbf{Q} , then the IP motion is given by

$$\begin{aligned} y_{\text{ip}} &= \mathbf{Q}_{\text{ip}} \cdot \mathbf{Y} - R_{33}Y_1 \\ &= \mathbf{Q}'_{\text{ip}} \cdot \mathbf{Y} \end{aligned} \quad (\text{I.2})$$

where the term $-R_{33}Y_1$ effectively centres the beam at the centre of the first magnet.

\mathbf{Q}'_{ip} is simple the vector \mathbf{Q}_{ip} with $-R_{33}$ added to the first element. The variance of the IP motion is then given as before (see equation 4, section 2.2)

$$\sigma_{y,\text{ip}}^2 = \mathbf{Q}_{\text{ip}}^T \cdot \mathbf{V}_Y \cdot \mathbf{Q}_{\text{ip}} \quad (\text{I.3})$$

Figure I.1 shows the RMS response function¹⁰ calculated for the TESLA BDS. Below $k \approx 1 \text{ m}^{-1}$, ($\lambda \approx 6 \text{ m}$), the response drops of approximately like k^3 . At short wavelengths, the value tends around ~ 1 which is dominated by the final doublet magnets (parallel-to-point focusing.)

⁹ For our ATL analysis, this was effectively achieved by choosing our z origin at the entrance to the beamline.

¹⁰ Note that this differs from the response function quoted in the literature [see 1], which normally show the variance response function, and so is the square of the result shown in figure I.1.

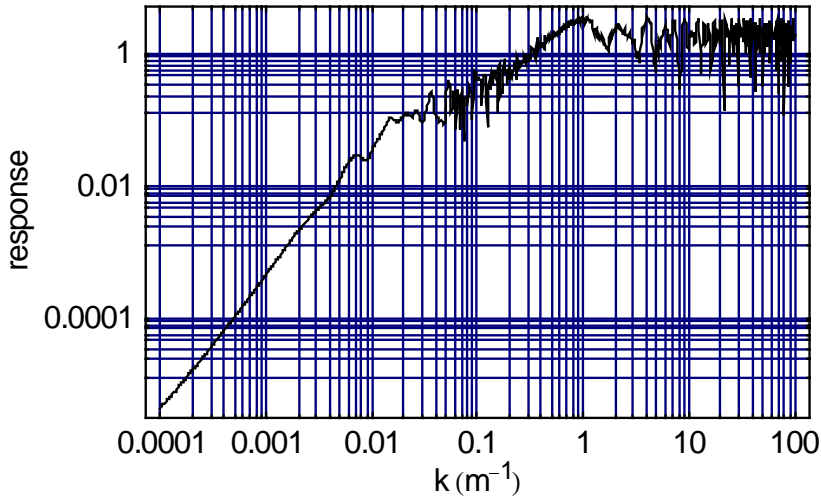


Figure I.1: IP offset response function. The response is effectively the ratio of IP beam motion to ground (quadruple) motion (see text for details.)

In a similar manor, we can calculate the response function for dispersion, the results of which are shown in figure I.11.

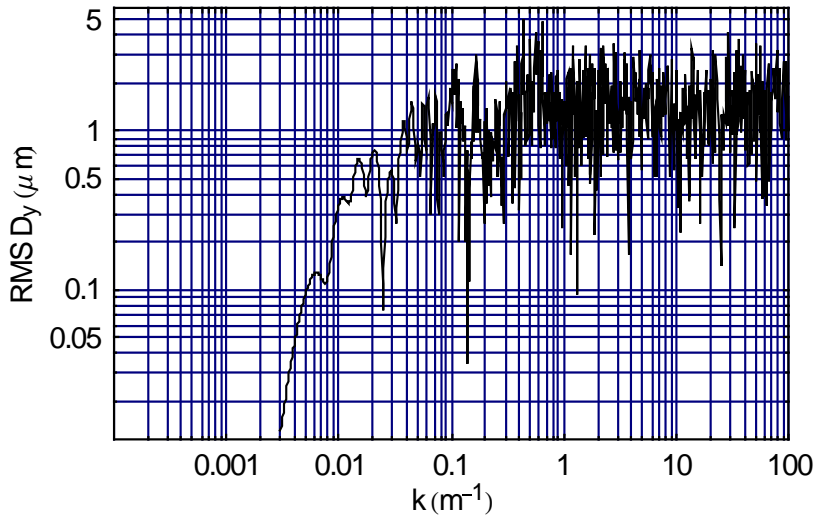


Figure I.2: Vertical IP dispersion response function scaled for an RMS amplitude of 70 nm.

In this case, we have scaled the response function to show the RMS IP vertical dispersion for a motion amplitude of 70 nm. We see that above $k \approx 1 \text{ m}^{-1}$ the RMS oscillates rapidly about the value calculated for random quadrupole motion in section 2.2.1 ($1.7 \text{ } \mu\text{m}$). Taking the velocity of sound as $\sim 6000 \text{ ms}^{-1}$, a frequency of 2 Hz corresponds to $k \approx 0.002 \text{ m}^{-1}$, which is well below the cut-off in figure I.2. If we consider that the amplitude of motion drops rapidly with increasing frequency, we can say that the major contribution to the dispersion is likely to be from waves in the 0.002-0.02 range (2-20 Hz). Hence from figure I.2 we can immediately see that our estimate for the generated dispersion based on *uncorrelated* 70 nm motion is likely to be very pessimistic.

Appendix II V_Y due to ATL-like ground motion

We first assume that we have an arbitrary origin $z = 0$, from which the distances to all the magnets ($z_i > 0$) are measured. If the motion of the i^{th} magnet relative to the origin is Y_i , then the variance of the relative motion between *two* magnets ($Y_i - Y_j$) is given by

$$\langle (Y_i - Y_j)^2 \rangle = \langle Y_i^2 \rangle + \langle Y_j^2 \rangle - 2\langle Y_i Y_j \rangle \quad (\text{II.1})$$

Assuming that all motion is governed by the ATL law, we can immediately express equation II.1 as

$$\begin{aligned} AT|z_i - z_j| &= ATz_i + ATz_j - 2\langle Y_i Y_j \rangle \\ \Leftrightarrow \langle Y_i Y_j \rangle &= \frac{1}{2} AT(z_i + z_j - |z_i - z_j|) \end{aligned} \quad (\text{II.1})$$

By examining the two possible cases of $z_i > z_j$ or $z_j > z_i$, we can show that

$$\langle Y_i Y_j \rangle = ATz_i, \text{ where } z_i < z_j \quad (\text{II.3})$$

Thus we arrive at the form of the covariance matrix given by equation 7 in section 2.2.2:

$$\mathbf{V}_Y = A \cdot T \cdot \begin{pmatrix} z_1 & z_1 & z_1 & \dots \\ z_1 & z_2 & z_2 & \dots \\ z_1 & z_2 & z_3 & \dots \\ \vdots & \vdots & \vdots & \ddots \end{pmatrix} \quad (\text{II.4})$$

The *correlation* of the motion between two location is given by

$$r_{ij} = \frac{\langle Y_i Y_j \rangle}{\sqrt{\langle Y_i^2 \rangle \langle Y_j^2 \rangle}} = \sqrt{\frac{z_i}{z_j}}, \text{ for } z_i < z_j \quad (\text{II.5})$$

Appendix III Effects of second-order dispersion on the first- and second-order beam moments

If the second-order dispersion is η , then the RMS beam size is given by

$$\begin{aligned}\sigma_y^2 &= \langle (y + \eta\delta^2)^2 \rangle - \langle y + \eta\delta^2 \rangle^2 \\ &= \langle y^2 \rangle + \eta^2 \langle \delta^4 \rangle - \eta^2 \langle \delta^2 \rangle^2\end{aligned}\tag{III.1}$$

assuming that $\langle y \rangle = 0$ and there is no initial correlation between y and δ . For a Gaussian distribution for the momenta (δ), we have $\langle \delta^4 \rangle = 3\langle \delta^2 \rangle^2$, and (III.1) becomes

$$\sigma_y^2 = \langle y^2 \rangle + 2\eta^2 \langle \delta^2 \rangle^2\tag{III.2}$$

The RMS contribution to the beamsize due to second-order dispersion (added in quadrature) is therefore given by $\sqrt{2}\eta\delta_{rms}^2$, or $\sqrt{2}$ times the centroid shift ($= \eta\delta_{rms}^2$).

References

1. A. Sery and O. Napoly, Phys. Rev. E., vol. 53, no. 5 (pp 5323-5337) (1996)
2. Andrei Seryi and Tor Raubenheimer, SLAC-PUB-8595, LINAC2000-MOA13 (2000)
3. R. Assmann, B. Jeanneret, A. Verdier, L. Vos, E. Wildner, F. Zimmermann, R. Brinkmann, C. Montag, I. Reyzl, N. Walker, C. Adolphsen, J. Frisch, N. Phinney, T. Raubenheimer, A. Seryi, and P. Tenenbaum, CERN-SL-2000-059-OP, CLIC-NOTE-448, Jun 2000, proceedings EPAC 2000 (2000)
4. TESLA Conceptual Design Report, DESY 1997-048, ECFA-1997-182 (1997)
5. B. A. Baklakov, P. K. Lebedev, V. V. Parkhomchuk, A. A. Sery, A. I. Sleptsov, and V. D. Shiltsev, INP Report 91-15, (1991)
6. R. Brinkmann, N. Walker, O. Napoly, and J. Payet, DAPNIA-SEA-00-04, CERN-OPEN-2000-227, proceedings EPAC 2000 (2000)
7. I. Reyzl, Proceedings of EPAC2000, WEOAF203 (2000)
8. V. Shiltsev, B. Baklakov, P. Lebedev, C. Montag, and J. Rossbach, DESY-HERA-95-06 (1995)
9. C. Montag, *private communication*
10. C. Montag, Nucl.Instrum. Meth. A378:369-375 (1996)
11. *The MERLIN-II C++ Class Library*, <http://www.desy.de/~njwalker/MerlinII>